J Therm Anal Calorim (2011) 104:707–716
DOI 10.1007/s10973-010-0971-x

Thermal and microstructural analysis of Cu(II) 2,2′-dihydroxy azobenzene and thin films deposition by MAPLE technique

C. Constantinescu · E. Morîntale · Ana Emandi · Maria Dinescu · P. Rotaru

Received: 2 June 2010 / Accepted: 16 July 2010 / Published online: 9 August 2010

Abstract A newly synthesized copper-complex exhibiting nonlinear optical properties, crystalline nature, and generating interest as a material for non-linear optical applications was investigated. As thermal stability studies are indispensable before attempting any laser-assisted processing experiments, the thermal behavior of 2,2′-dihydroxy azobenzene with Cu^{2+} cations that are found to organize themselves as non-central symmetric crystallites, was investigated. The thin films were deposited on silicon substrates by matrix-assisted pulsed laser evaporation using a Nd:YAG laser working at 266 and 355 nm. Thermal analysis of the bulk compound indicates a higher thermal stability in argon flow when compared to the air atmosphere; as well, since, the adhesion of the compound onto the substrate enhances the bonding, the thermal stability of the Cu complex increases. Fourier transform infrared spectroscopy, atomic force microscopy, scanning electron microscopy, spectroscopic ellipsometry, and ultraviolet–visible spectroscopy investigations were also performed.

Keywords Cu complex · MAPLE · Thermal analysis · Thin film

C. Constantinescu · M. Dinescu
PPAM-Lasers Department, INFLPR-National Institute for Laser, Plasma and Radiation Physics, 409 Atomistilor blvd., Magurele, 077125 Bucharest, Romania

E. Morîntale · P. Rotaru (✉)
Faculty of Physics, University of Craiova, 13 AI Cuza Street, 200585 Craiova, Dolj, Romania
e-mail: protaru@central.ucv.ro; petrerotaru@yahoo.com

A. Emandi
Department of Inorganic Chemistry, Faculty of Chemistry, University of Bucharest, 23 Dumbrava Rosie Street, 010184 Bucharest, Romania

Introduction

Metal-organic complex compounds with azobenzene rings are important materials of real economic interest, with direct applications as thin films for non-linear optics, optical storage, or for various sensors [1–4]. Laser processing of such complex materials represents a solution for obtaining smooth, continuous, and chemically intact thin films. Unfortunately, conventional pulsed laser deposition (PLD)—which has been used as a successful technique for fabricating inorganic thin films of controlled thickness and composition [5]—cannot be applied to most organic and other soft materials, since irradiation by UV light induces substantial decomposition of the target molecules [6–10]. Thin films of organometallic and coordinative compounds, polymers, bio- and hybrid metal-organic materials can be fabricated employing an alternative technique, known as MAPLE (matrix assisted pulsed laser evaporation) [11–13]. This recent technique is a versatile way of depositing such fragile compounds on various surfaces and controlling shape and thickness at nanometer scale (10–500 nm) [14–28]. MAPLE involves dissolving or suspending the complex material (0.1–2 wt%) in a volatile solvent (matrix), freezing the mixture to create a solid target, and employing a low-fluence pulsed laser to displace the target and pulverize it into vacuum chamber. When the matrix is irradiated by laser radiation, the solvent evaporates, whereas the guest molecules are collected onto a substrate. A successful film deposition by MAPLE technique requires a matrix with an absorption band in the range of the working wavelength of the laser and a relatively low absorption by the guest material. It is also important to consider that possible photochemical reactions between the matrix and guest materials should be avoided or considerably reduced, but these requirements are usually difficult to fulfill completely.

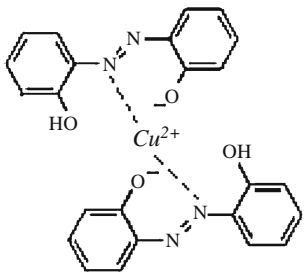

Fig. 1 Molecular formula of the $Cu(DAB)_2$ complex

This article analyzes the bulk and the thin films of Cu(II) 2,2′-dihydroxy azobenzene—$Cu(DAB)_2$ (Fig. 1)—a potential candidate for such applications described above, by several structural and morphological investigation techniques. Thermal analyses of new azoderivatives, used as precursors for reduced-scale materials synthesis [29–31], biological active materials [32–37], or designed for temperature-controlled applications like dyes [38–41] exhibiting liquid-crystalline nature [42–48], are needed before functionalizing them [4, 17, 49–53]. TA was performed on $Cu(DAB)_2$ to establish its stability and physico-chemical transformations as a function of temperature. These investigations are needed to fully understand the behavior of the structure [24] and for further comparing whether TA data from the bulk and those from the thin films exhibit similarities [54].

Experimental

Preparation of $Cu(DAB)_2$ material

The copper metal-organic complex $Cu(DAB)_2$ was obtained in laboratory, starting from a hot solution of ligand (2,2′-dihydroxy azobenzene, 0.6 mM) in ethanol, mixed with a solution of copper (II) chloride (hydrated copper chloride, 1.2 mM) in ethanol; the mixture was subsequently stirred and refluxed for 1.5 h in a water bath until the complex gets precipitated. The pH of the solution was adjusted with ammonia solution up to 7–7.5 during the reaction. A fine crystalline product was separated by cooling the solution; this was filtered, re-crystallized, and then washed with ethanol. Further information on the procedure of $Cu(DAB)_2$ synthesis may be found elsewhere [4, 55].

Thin film obtaining by MAPLE technique

The target was prepared by dissolving $Cu(DAB)_2$ crystals in toluene, at a concentration of 1% wt. For each target we used, 1 mL of solution was poured onto the target holder using a micropipette. The target holder was cooled by gently immersing it into liquid nitrogen (boiling point: 77 K), until the solution has frozen (toluene freezing point: 180.16 K). Subsequently, the target holder was mounted in its place inside the deposition chamber, where it reached 143 ± 5 K—the working temperature throughout the deposition procedure. The substrates were cleaned in an ultrasonic bath for 15 min, using acetone and isopropanol as cleaning media; the substrates were subsequently dried under (pressured) nitrogen gas. For the MAPLE experiments, during which the $Cu(DAB)_2$ thin films presented in this article were obtained, a laser beam from a "Surelite II" pulsed Nd:YAG laser system ("Continuum Company," 266 and 355 nm wavelength, 7 ns duration of the pulse, 10 Hz) was focused on the $Cu(DAB)_2$ frozen target, with a spot area of 1.6 mm^2 and a fluence of 0.4 J cm^{-2} (this value was chosen after a series of trials, as being the best fluence to preserve $Cu(DAB)_2$ structure). Eight depositions were performed on silicon: four at $\lambda = 355$ nm, and four at $\lambda = 266$ nm. The number of pulses ranged from 5,000 to 42,000 (from 8 to 70 min). In order to have uniform evaporation, the laser beam scanned the target, while the target was kept refrigerated in continuous flow of liquid nitrogen and rotated with a motion feed-through of 20 rotations min^{-1} driven by a motor. For controlling the temperature, two thermocouples were placed in two different spots of the target holder. The depositions took place in vacuum, with a background pressure ranging from 1×10^{-4} to 4×10^{-4} mbar during the depositions [15] and a base pressure of 4.5×10^{-5} mbar before the laser irradiation; we have used a "Pfeiffer-Balzers TPU 170" turbo-molecular pump (170 L s^{-1} volume flow rate). Detailed information about MAPLE experimental setup is presented elsewhere [15–18].

Characterization techniques for bulk and thin films

The $Cu(DAB)_2$ bulk material was characterized by means of Fourier transform infrared spectroscopy (FTIR), scanning electron microscopy (SEM), ultraviolet–visible spectroscopy (UV–Vis), and light polarized optical microscopy (LPOM). Thin films obtained by MAPLE were characterized by atomic force microscopy (AFM) and spectroscopic-ellipsometry (SE). Both $Cu(DAB)_2$ bulk and thin films were analyzed by TA techniques.

Chemical bonding of the $Cu(DAB)_2$ bulk sample was investigated by FTIR with a "PerkinElmer SPECTRUM 100" spectrometer in the wavenumber range of 650–4000 cm^{-1}. All spectra were obtained using universal attenuated total reflectance (UATR) accessory, at a resolution of 4 cm^{-1}, with 4 scans, and CO_2/H_2O correction. SEM measurements were performed on the $Cu(DAB)_2$ crystals using a "FEI Inspect F" setup. The electron acceleration voltage was set between 200 V and 30 kV; the lateral resolution was ~2 nm.

Thermal analysis measurements (TG, DTG, and DSC) of the $Cu(DAB)_2$ complex were carried out in dynamic air and argon atmospheres (150 cm^3 min^{-1}), under non-isothermal linear regimes, using a horizontal "Diamond" Differential/Thermogravimetric Analyzer from PerkinElmer Instruments. Samples from 0.5 to 3 mg, contained in aluminium crucibles, were heated in the temperature range of 20–600 °C. The employed heating rates were: 2, 4, 6, 8, and 10 K min^{-1}. An optical microscope "LEICA DM 2500P" working under polarized light (90° crossed polarizers) was used to observe morphological transformations during heating. The last was performed on a "TMS 94 Linkam Scientific Instrument Ltd." heating table at a rate of 2 K min^{-1}.

Thin films surface aspect and roughness of several different areas and dimensions were analyzed using AFM technique with a "Park XE-100" setup produced by "Park Systems." The scans were made in non-contact mode, using a silicon carbide tip (10-nm radius of curvature). SE measurements were performed by using a "Woolam Vertical Variable Angle Spectroscopic Ellipsometer" (W-VASE), equipped with a high pressure Xe discharge lamp incorporated in an HS-190 monochromator, in the visible and near-UV region of the spectrum at wavelengths between 250 and 1350 nm, step of 10 nm, at 60° and 65° angles of incidence.

Results and discussion

Structural and morphological characterization of $Cu(DAB)_2$

The FTIR spectrum of the free ligand (2,2′-dihydroxy azobenzene = DAB) reveals intense specific bands at 3320, 1590, 1470, 1140, and at 745 cm^{-1}, which are related to –N=N–, –C=C– aromatic ring, C–N=, kelatic –OH, and phenolic –OH, respectively. The FTIR spectrum for $Cu(DAB)_2$ is presented in Fig. 2, and the characteristic absorption bands for the individual groups are shown in Table 1; the typical bands are related to –N=N–, which gives a signal that is split and becomes maximum around 1588 cm^{-1}, and phenolic –OH that is shifted to 1259 cm^{-1} after complexation. The kelatic band at 3056 cm^{-1} is unaffected within the complex, and the bands corresponding to the coordinated water molecules are absent. These results show that the ligand binds the metal by the azo group and by one –OH group that is shifted to 1259 cm^{-1} after complexation, while the other gives the unaffected band at 3056 cm^{-1}. The most intense absorption bands of $Cu(DAB)_2$, identified in the IR spectrum, were attributed to the following chemical bonding:

- Absorption lines at 744, 757, 1177–1259, 1466 and at 1588 cm^{-1} are related to ortho-substituted aromatic compounds.
- Absorption lines at 744, 757, 1034, 1177, 1203, 1216, 1259, 1452, 1466, 1568, 1588, 3167, 3247, and at 3314 cm^{-1} are related to hydroxy- or amino-substituted aromatic compounds.
- Absorption lines at 744, 757, 843, 876, 1143, 1177, 1203, 1216, 1259, 1341, 1466, 1568, 1588, 3167, 3274, and at 3314 cm^{-1} are related to ortho-substituted aromatic compounds by hydroxyl and azo groups.

These peaks were particularly analyzed, as they permit a comparison of the thin films to the bulk material, to detect whether the deposition parameters preserved the stoichiometry of the samples.

In Fig. 3 we can be observe the microstructural image of the $Cu(DAB)_2$ powder; short acicular crystals form, typical for such compounds, which are disposed in a compact array. The crystals are between 8 and 11 μm in length, and between 1.5 and 3 μm thick.

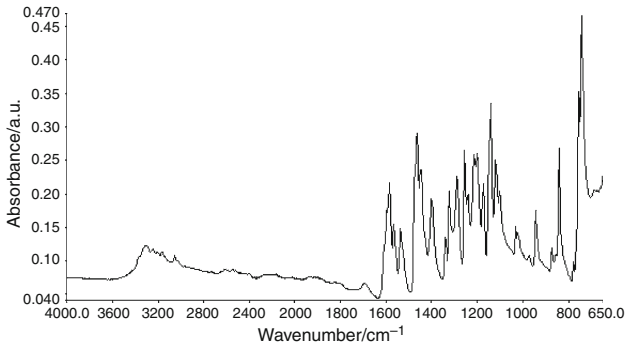

Fig. 2 FTIR spectrum of the $Cu(DAB)_2$ complex

Thermal analysis of $Cu(DAB)_2$

Thermal analysis techniques are frequently used to determine the thermal stability and molecular structure of metal-organic compounds [24, 36, 37, 56–58]. The thermal stability of the $Cu(DAB)_2$ complex determined by TA measurements, as well as the thermal effects, can be observed in the TG, DTG, and DSC curves in air (Fig. 4), and argon (Fig. 5) dynamic atmospheres.

In both cases, the system loses ~3% of its mass, most probably corresponding to the crystallization solvent.

Decomposition in air and argon of the copper complex takes place in two main steps. For the case of the decomposition in air, by looking at the thermal effects, the first step is slightly endothermic (with incommensurable exchanged heat), while the second step is highly exothermal. In Table 2, the enthalpy variations of the system during the (second step)

Table 1 Characteristic absorption bands for the individual groups of the $Cu(DAB)_2$ complex

Wavenumber /cm^{-1}	Intensity[a]	Assignments
3314	m	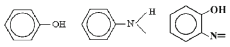
3247	m	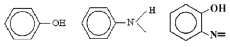
3167	m	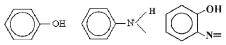
3056	w	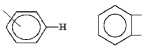
1588	s	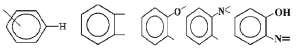
1568	m	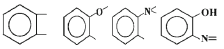
1538	m	
1466	vs	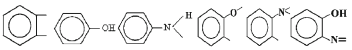
1452	m	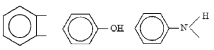
1401	m	
1341	w	
1326	m	
1290	m	
1259	m	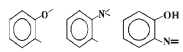
1216	m	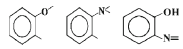
1203	m	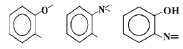
1177	m	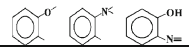
1143	vs	
1122	m	
1104	m	
1034	w	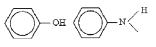
947	m	
876	w	
843	s	
757	vs	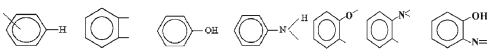
744	vs	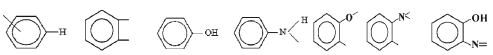

[a] *vs* very strong, *s* strong, *m* medium, *w* weak

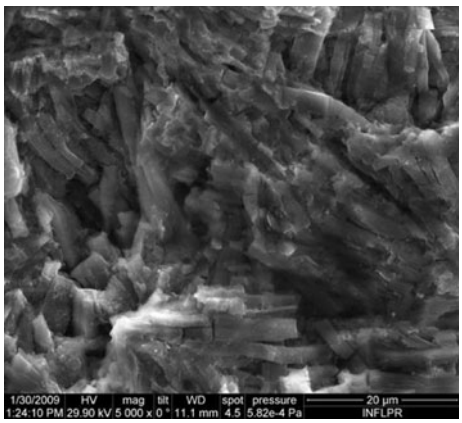

Fig. 3 SEM image of the $Cu(DAB)_2$ bulk

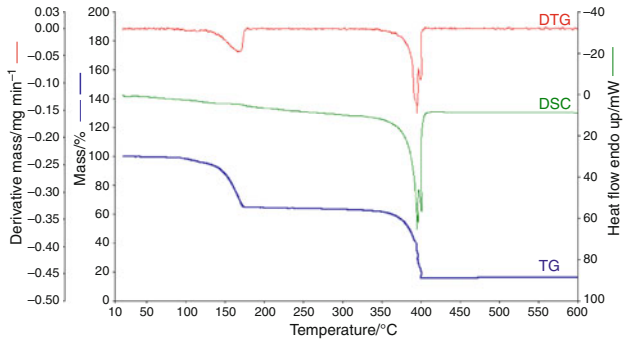

Fig. 4 Thermoanalytical curves for the $Cu(DAB)_2$ complex in air at $\beta = 10$ K min^{-1}

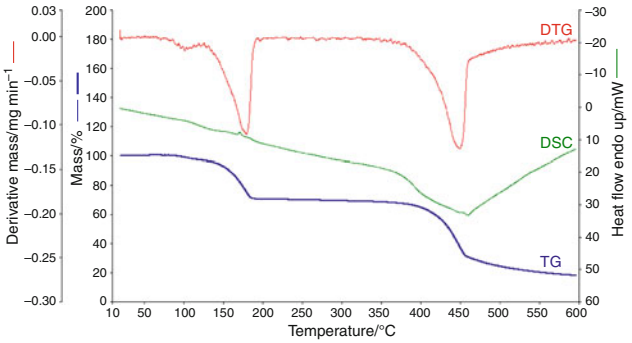

Fig. 5 Thermoanalytical curves for the $Cu(DAB)_2$ complex in argon at $\beta = 10$ K min^{-1}

oxidative decomposition in air at different heating rates are presented.

A displacement to higher temperature for the temperature range of the process was observed, when increasing the heating rate. The thermal effect of the second stage is exothermal and extremely powerful (more than $-14{,}500 \pm 1{,}000$ kJ kg^{-1}) for all heating rates; when reaching 395 °C,

Table 2 The thermal effect of the second-step oxidative decomposition in air

β/K min^{-1}	Temperature range/°C	Peak maximum/°C	$\overline{\Delta H}$/kJ kg^{-1}
2	306–347	344.4	−14,500
4	311–367	362.2	
6	327–381	374.0	
8	333–390	382.1	
10	359–399	391.3	

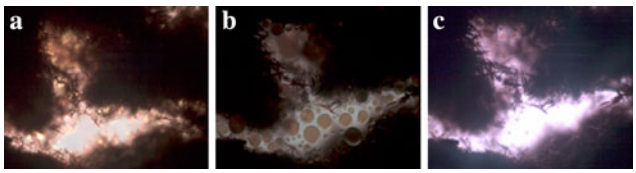

Fig. 6 Optical images of the $Cu(DAB)_2$ complex during the first stage of decomposition

the compound decomposes almost instantaneously (Fig. 4, TG curve).

The first step of decomposition was also observed by optical microscopy, in a way similar to the one described in the literature [17, 59]. The optical micro-images from Fig. 6 were recorded on a polarizing microscope LEICA DM 2500 P, equipped with a video-recorder camera and a hot thermostated stage TMS 94 (Linkam Scientific Instruments Ltd.) connected to the temperature programmer. The compound was introduced between two parallel glass plates (a slide and a coverslip) without any particular care and was examined between crossed polarizers under a polarizing microscope. Figure 6a reveals the solid sample before decomposition, Fig. 6b is an image that shows the gas formation, while the copper complex is decomposing, and Fig. 6c was recorded at 210 °C after the first decomposition step ended.

Decomposition of the copper complex in argon consists of two steps as well. The first step is slightly endothermic, while the second one is slightly exothermal (because there is no oxygen present in the gas flow). The first decomposition step recorded in argon atmosphere takes place in the same manner as the decomposition recorded in air flow, up to ~175 °C (for the 10 K min^{-1} experiments). The second decomposition process starts at 400 °C, exactly the temperature where in the air flow was noticed the spontaneous reaction. This explains as to why in the air flow case, the process starts at lower temperatures, enhanced by the presence of oxygen in the gas flow. From 450 °C, the mass profile changes which is due to the shift of the first part of the reaction to higher temperatures in the absence of the oxygen. The mass losses at the extreme values of the

Table 3 The gravimetric effect of the decomposition in air and in argon at 600 °C

β/K min^{-1}	Air		Argon	
	Mass loss/%	Residue/%	Mass loss/%	Residue/%
2	84.12	15.88	78.25	21.75
10	84.48	15.52	81.93	18.07

heating rates during the decomposition of the complex, in air and in argon, are presented in Table 3.

As can be seen from Table 3, and from the TG curve in Fig. 5, the thermal decomposition finishes up to 600 °C in the case of argon flow experiment. When decomposing the copper complex in air flow, the experimental values for the mass loss approach, the theoretical value of 16.23% that is related to a CuO residue. The experimental mean mass loss of 84.3% is larger than the theoretical value of 83.76%, and this can be related to copper loss to the gas phase during the copper complex decomposition, to the formation of small amounts of Cu_2O, or even to metal formation [60] (sometimes, the crucible had the characteristic color of metallic copper).

For the decomposition in argon flow, the experimental values of the mass for the residue at 600 °C are higher than the theoretical value, for both heating rates; this phenomenon augments at lower heating rates. As the decomposition in argon is not oxidative, the carbon that forms during the copper complex decomposition does not burn; hence, it is slowly lost.

Thermal analysis of $Cu(DAB)_2$ thin film deposited by MAPLE technique on silicon substrates was also performed in air, for the heating rate of 10 K min^{-1} using the same thermoanalytical instrument. For all the analyzed MAPLE-deposited samples, the gravimetric effect was insignificant because of the small amount of deposited $Cu(DAB)_2$ in comparison to the huge amount of silicon substrate. In terms of thermal effects, only for the sample irradiated with 30,000 laser pulses (for 266-nm laser wavelengths used), a weak exothermal effect (−0.11 kJ kg^{-1}) was identified on the DSC diagram (Fig. 7). It corresponds to the strong exothermal effect in the bulk material (second thermogravimetric process in Fig. 4). This thermal effect on the thin film can be observed because of the very high enthalpy value (−14,500 kJ kg^{-1}) of the exothermal process of only $Cu(DAB)_2$ bulk material.

The exothermal effect observed in the thin film ($Cu(DAB)_2$ deposited on the silicon substrate appears to be relatively minor ($\sim 10^5$ times smaller than for the pure $Cu(DAB)_2$ compound). This is due to the actual amount of the deposited material which is itself extremely small: only a few nanograms of $Cu(DAB)_2$ deposited on a 3 × 3 mm^2 area of silicon substrate (a few milligrams) used for the

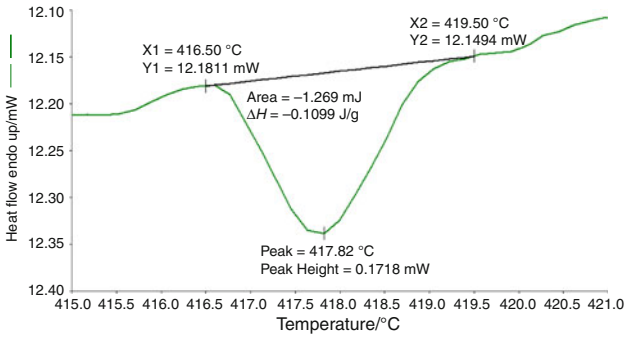

Fig. 7 The thermal effect of oxidative decomposition in air of a thin-film sample, at 10 K min^{-1}

thermal analysis. The small amount of dispersed complex on the substrate and eventually its good adhesion provides to the compound a higher thermal stability, and shifts the temperature of thin film oxidative decomposition at a higher values (T_{peak} = 417.8 °C)—comparing with the lower temperatures (T_{peak} = 391.3 °C) for the bulk $Cu(DAB)_2$ thermal decomposition.

The results show that for samples deposited at 266-nm laser wavelength, the copper complex deposited by MAPLE has no damage to the chemical structure, while for other samples it appears to have suffered some modifications: this is possibly due to stronger laser interaction with the compound because of weaker protection by the matrix during the deposition procedure at 355 nm laser wavelength, which leads to $Cu(DAB)_2$ structure alteration; UV–Vis spectroscopy supports this fact.

The UV–Vis spectra of toluene (matrix) and $Cu(DAB)_2$ are presented in Fig. 8; it can be easily observed that toluene absorbs better at 266 nm and weaker at 355 nm, with respect to $Cu(DAB)_2$. The procedure was necessary in order to establish such absorption characteristics of the $Cu(DAB)_2$ and its toluene matrix at selected wavelengths, to subsequently correlate thin film properties with the laser influence on the target material during deposition.

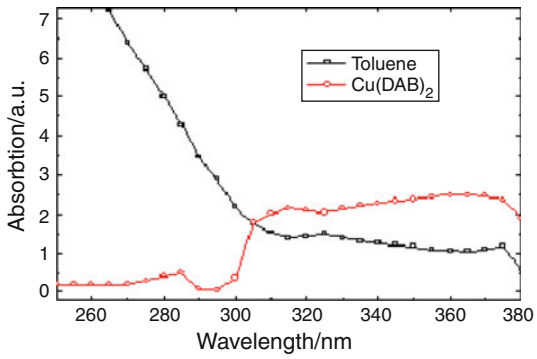

Fig. 8 UV–Vis spectra of toluene and of the $Cu(DAB)_2$ complex

For the thin-film samples deposited at 266-nm laser wavelength, the copper complex was deposited with virtually no damage to the chemical structure, while for the samples deposited at 355 nm it appears that some modifications occurred; this is possibly due to laser radiation interacting with the compound because of weaker protection by the matrix during the deposition procedure at 355-nm laser wavelength that leads to slight structure alteration in $Cu(DAB)_2$, since the complex has higher absorption at this wavelength; organic compounds with a high degree of conjugation are known to absorb light in the near-UV region of the electromagnetic spectrum [61].

Atomic force microscopy and spectroscopic ellipsometry of thin films

Visually, the samples appear uniform and completely covered (Fig. 9). The AFM images of the same sample deposited at 266-nm laser wavelength revealed a continuous and smooth surface covering the entire exposed area of the substrate. Although several areas of the samples were scanned by AFM, only three significant images of the samples were chosen, presented in Fig. 9 at different scanned areas: 20 × 20 μm^2 (a), 10 × 10 μm^2 (b), and 5 × 5 μm^2 (c). The samples were deposited at a fluence of 0.4 J cm^{-2} (50 min/30,000 laser pulses), and have a roughness (as root mean square value, or RMS) of about 20.1–25.8 nm. No droplets are present, and substrate types do not influence the morphology of the films.

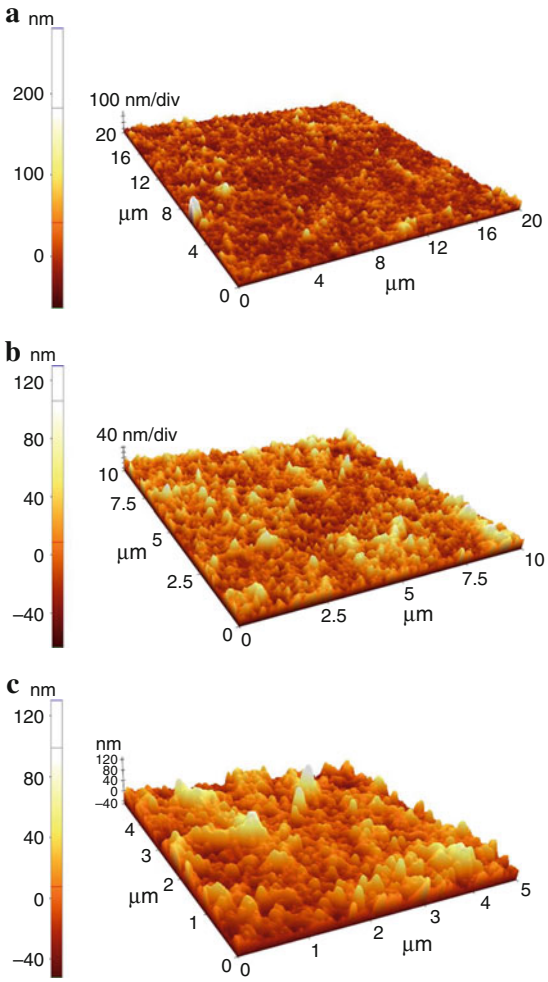

Fig. 9 AFM images of the $Cu(DAB)_2$ samples deposited on silicon, at different scanning areas: 20 × 20 μm^2 (**a**), 10 × 10 μm^2 (**b**), and 5 × 5 μm^2 (**c**)

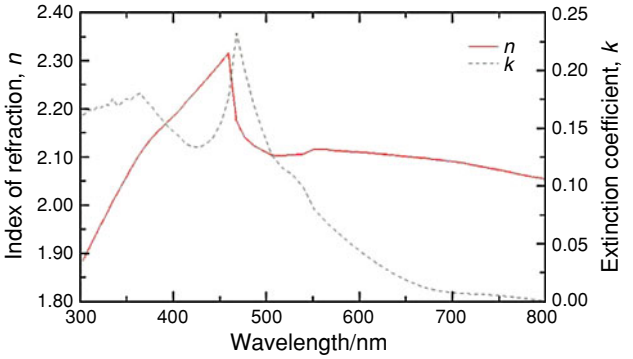

Fig. 10 The refractive and the extinction indexes of the $Cu(DAB)_2$ complex, determined from the Cauchy optical constants

Since the AFM measurements indicate smooth and continuous thin films, it was possible to employ SE in order to determine the characteristic thickness and roughness (data are presented in Fig. 10). The optical model was built-up to fit the experimental data in a four-layer configuration: silicon, native silicon oxide (3 nm), $Cu(DAB)_2$, and a "roughness layer"; the roughness-layer was approximated as a 50% $Cu(DAB)_2$ and 50% air. The optical constants used to fit the silicon and silicon oxide layers are from the literature [62], while the $Cu(DAB)_2$ thin film was fitted as a layer that fulfils the Cauchy–Urbach formalism (weak absorption in the visible region of the spectrum).

The first step was to approximate $Cu(DAB)_2$ thin-film thickness and the constants in the formalism, followed by the determination of the refraction (n) and extinction indexes (k) by normal Cauchy–Urbach "point by point" fitting of the spectra; detailed information of the setup, of the mathematical models, and formulas used for fitting the experimental data are presented in [63]. The SE investigations were performed between 250- and 1700-nm wavelength, although only the 300–800-nm interval was considered here; thin film thicknesses varied from 101 to 310 nm (±12 nm) and the RMS from 12 to 21 nm, depending on the number of laser pulses. At 550 nm-wavelength, the samples exhibit a refractive index of 2.11 ± 0.21 and an extinction index of 0.13 ± 0.013; value error is related to mathematical model used in fitting the experimental data, to possible thin-film discontinuities,

e.g., small bubbles, or to the existence of a small slope in the thin-film surface structure.

Conclusions

Thermal analysis of Cu(II) 2,2′-dihydroxy azobenzene organo-metallic compound was performed to establish its chemical and physical transformations and thermal stability. MAPLE technique was used to obtain thin films of this hybrid material. The results indicate the preservation of the initial compound structure on the substrate, for the samples deposited by MAPLE to be better at 266 nm laser wavelength than at 355 nm. TA of the bulk compound indicates a higher thermal stability in argon flow when compared with the air atmosphere and a different decomposition pathway for the second step. As well, since the adhesion of the compound onto the substrate enhances the bonding, the thermal stability of the Cu complex increases when dispersed on the Si layers. AFM images reveal continuous and smooth surfaces for the deposited thin films of $Cu(DAB)_2$ obtained on silicon substrate. The modeling of SE data indicates thicknesses ranging from 101 to 310 nm, depending on the deposition conditions, and a refractive index of 2.11 (at 550-nm wavelength).

Acknowledgements The authors acknowledge the support of I. Goldner, A. Rotaru, V. Ion, A. Moldovan, and C. Luculescu, for their help during the investigation experiments. We thank Mr. Ion "Felix" Nistorescu for his help during the thin-film deposition experiments.

References

1. Qiu FX, Zhang W, Yang DG, Zhao MJ, Cao GR, Li PP. Synthesis, characterization, and thermo-optical properties of azobenzene polyurethane containing chiral units. J Appl Polym Sci. 2010;115:146–51.
2. Chiarelli PA, Liu DG, Watkins EB, Trouw FR, Majewski J, Casson JL, Tang ZX, Johal MS, Robinson JM, Wang HL. Molecular order in Langmuir–Blodgett assembled films of an azobenzene amphiphile. Thin Solid Films. 2009;517:4638–43.
3. Nishihara H. Combination of redox- and photochemistry of azo-conjugated metal complexes. Coord Chem Rev. 2005;249:1468–75.
4. Constantinescu C, Emandi A, Vasiliu C, Negrila C, Logofatu C, Cotarlan C, Lazarescu M. Thin films of Cu(II)-*o*,*o*′-dihydroxy azobenzene nanoparticle-embedded polyacrylic acid (PAA) for nonlinear optical applications developed by matrix assisted pulsed laser evaporation (MAPLE). Appl Surf Sci. 2009;255:5480–5.
5. Eason RW. Pulsed laser deposition of thin films. New York: Wiley; 2007.
6. Rau H. Photoisomerization of azobenzenes. Photoreactive organic thin films. San Diego: Academic Press; 2002.
7. Lippert T, Dickinson J. Chemical and spectroscopic aspects of polymer ablation: special features and novel directions. Chem Rev. 2003;103:453–85.
8. Sudesh Kumar G, Neckers D. Photochemistry of azobenzene-containing polymers. Chem Rev. 1989;89:1915–25.
9. Xie S, Natansohn A, Rochon P. Recent developments in aromatic azo polymers research. Chem Mater. 1993;5:403–11.
10. Rusu E, Dorohoi D, Airinei A. Solvatochromic effects in the absorption spectra of some azobenzene compounds. J Mol Struct. 2008;887:216–9.
11. McGill RA, Chung R, Chrisey DB, Dorsey PC, Matthews P, Pique A, Mlsna TE, Stepnowski JL. Performance optimization of surface acoustic wave chemical sensors. IEEE Trans Ultrason Ferroelectr Freq Control. 1998;45:1370–80.
12. Pique A, McGill RA, Chrisey DB, Leonhardt D, Mlsna TE, Spargo BJ, Callahan JH, Vachet RW, Chung R, Bucaro MA. Growth of organic thin films by the matrix assisted pulsed laser evaporation (MAPLE) technique. Thin Solid Films. 1999;355–356:536–41.
13. Chrisey DB, Pique A, McGill RA, Horwitz JS, Ringeisen BR, Bubb DM, Wu K. Laser deposition of polymer and biomaterial films. Chem Rev. 2003;103:553–76.
14. Leveugle E, Zhigilei LV, Sellinger A, Fitz-Gerald JM. Computational and experimental study of the cluster size distribution in MAPLE. Appl Surf Sci. 2007;253:6456–60.
15. Houser E, Chrisey D, Bercu M, Scarisoreanu N, Purice A, Colceag D, Constantinescu C, Moldovan A, Dinescu M. Functionalized polysiloxane thin films deposited by MAPLE for advanced chemical sensor applications. Appl Surf Sci. 2006;252:4871–6.
16. Constantinescu C, Scarisoreanu N, Moldovan A, Dinescu M, Vasiliu C. Thin films of polyaniline deposited by MAPLE technique. Appl Surf Sci. 2007;253:7711–4.
17. Rotaru A, Constantinescu C, Rotaru P, Moanta A, Dumitru M, Socaciu M, Dinescu M, Segal E. Thermal analysis and thin film deposition by MAPLE of a 4CN type azomonoether. J Therm Anal Calorim. 2008;92:279–84.
18. Lippert T, Chrisey D, Purice A, Constantinescu C, Filipescu M, Scarisoreanu N, Dinescu M. Laser processing of soft materials. Rom Rep Phys. 2007;59:483–98.
19. Bigi A, Boanini E, Capuccini C, Fini M, Mihailescu I, Ristoscu C, Sima F, Torricelli P. Biofunctional alendronate–Hydroxyapatite thin films deposited by matrix assisted pulsed laser evaporation. Biomaterials. 2009;30:6168–77.
20. Frycek R, Jelinek M, Kocourek T, Fitl P, Vrnata M, Myslik V, Vrbova M. Thin organic layers prepared by MAPLE for gas sensor application. Thin Solid Films. 2006;495:308–11.
21. Kopecky D, Vrnata M, Vyslouzil F, Myslik V, Fitl P, Ekrt O, Matejka P, Jelinek M, Kocourek T. Polypyrrole thin films for gas sensors prepared by matrix-assisted pulsed laser evaporation technology: effect of deposition parameters on material properties. Thin Solid Films. 2009;517:2083–7.
22. Constantinescu C, Palla-Papavlu A, Rotaru A, Florian P, Chelu F, Icriverzi M, Nedelcea A, Dinca V, Roseanu A, Dinescu M. Multifunctional thin films of lactoferrin for biochemical use deposited by MAPLE technique. Appl Surf Sci. 2009;255:5491–5.
23. Rotaru A, Kropidłowska A, Constantinescu C, Scarisoreanu N, Dumitru M, Strankowski M, Rotaru P, Ion V, Vasiliu C, Becker B, Dinescu M. CdS thin films obtained by thermal treatment of Cadmium (II) complex precursor deposited by MAPLE technique. Appl Surf Sci. 2009;255:6786–9.
24. Rotaru A, Constantinescu C, Mandruleanu A, Rotaru P, Moldovan A, Gyoryova K, Dinescu M, Balek V. Matrix assisted pulsed laser evaporation of zinc benzoate for ZnO thin films and non-isothermal decomposition kinetics. Thermochim Acta. 2010;498:81–91.
25. Rodrigo K, Toftmann B, Schou J, Pedrys R. Laser-induced ion emission during polymer deposition from a flash-frozen water ice matrix. Chem Phys Lett. 2004;399:368–72.
26. Purice A, Schou J, Kingshott P, Pryds N, Dinescu M. Characterization of lysozyme films produced by matrix assisted pulsed laser evaporation (MAPLE). Appl Surf Sci. 2007;253:6451–5.

27. Purice A, Schou J, Kingshott P, Dinescu M. Production of active lysozyme films by matrix assisted pulsed laser evaporation at 355 nm. Chem Phys Lett. 2007;435:350–3.
28. Sellinger A, Leveugle E, Fitz-Gerald JM, Zhigilei LV. Generation of surface features in film deposited by matrix-assisted pulsed laser evaporation: the effects of the stress confinement and droplet landing velocity. Appl Phys A. 2008;92:821–9.
29. Lucilha AC, Bonancea CE, Barreto WJ, Takashima K. Adsorption of the diazo dye Direct Red 23 onto a zinc oxide surface: a spectroscopic study. Spectrochim Acta A. 2010;75:389–93.
30. Foletto EL, Jahn SL, Moreira RDPM. Hydrothermal preparation of Zn_2SnO_4 nanocrystals and photocatalytic degradation of a leather dye. J Appl Electrochem. 2010;40:59–63.
31. Badea M, Olar R, Cristurean E, Marinescu D, Emandi A, Budrugeac P, Segal E. Thermal stability study of some azo-derivatives and their complexes—Part 2. New azo-derivative pigments and their Cu(II) complexes. J Therm Anal Calorim. 2004;77:815–24.
32. Olar R, Badea M, Marinescu D, Lazar V, Chifiriuc C. New complexes of Ni(II) and Cu(II) with Schiff bases functionalised with 1,3,4-thiadiazole: spectral, magnetic, biological and thermal characterization. J Therm Anal Calorim. 2009;97:721–7.
33. El-Tabl AS, Aly FA, Shakdofa MME, Shakdofa AME. Synthesis, characterization, and biological activity of metal complexes of azohydrazone ligand. J Coord Chem. 2010;63:700–12.
34. Olczak-Kobza M. Synthesis and thermal characterization of zinc(II) di(*o*-aminobenzoate) complexes of imidazole and its methyl derivatives. Thermochim Acta. 2004;419:67–71.
35. Haroun MA, Khirstova PK, Gasmelseed GA, Covington AD. Influence of oxazolidines and zirconium oxalate crosslinkers on the hydrothermal, enzymatic, and thermo mechanical stability of type 1 collagen fiber. Thermochim Acta. 2009;484:4–10.
36. Badea M, Olar R, Marinescu D, Segal E, Rotaru A. Thermal stability of some new complexes bearing ligands with polymerizable groups. J Therm Anal Calorim. 2007;88:317–21.
37. Olar R, Badea M, Stanica N, Cristurean E, Marinescu D. Synthesis, characterisation and thermal behaviour of some complexes with ligands having 1,3,4-thiadiazole moieties. J Therm Anal Calorim. 2005;82:417–22.
38. Rotaru A, Bratulescu G, Rotaru P. Thermal analysis of azoic dyes; Part I non-isothermal decomposition kinetics of [4-(4-chlorobenzyloxy)-3-methylphenyl](*p*-tolyl)diazene in dynamic air atmosphere. Thermochim Acta. 2009;489(1–2):63–9.
39. Rotaru A, Gosa M, Segal E. Isoconversional linear integral kinetics of the non-isothermal evaporation of 4-[(4-chlorobenzyl)oxy]-4′-trifluoromethyl-azobenzene. Studia Universitas Babeş-Bolyai Chemia. 2009;3:185–92.
40. Rotaru A, Moanta A, Popa G, Rotaru P, Segal E. Thermal decomposition kinetics of some aromatic azomonoethers. Part IV. Non-isothermal kinetics of 2-allyl-4-((4-(4-methylbenzyloxy) phenyl)diazenyl) phenol in dynamic air atmosphere. J Therm Anal Calorim. 2009;97(2):485–91.
41. Rotaru A, Kropidlowska A, Rotaru P. On the inappropriate fit of diffusion functions at thermal decomposition of some azomonoethers in liquid state. Phys AUC. 2007;17(2):115–8.
42. Gur M, Kocaokutgen H, Tas M. Synthesis, spectral, and thermal characterisations of some azo-ester derivatives containing a 4-acryloyloxy group. Dyes Pigment. 2007;72(1):101–8.
43. Badea M, Emandi A, Marinescu D, Cristurean E, Olar R, Braileanu A, Budrugeac P, Segal E. Thermal stability of some azo-derivatives and their complexes—1-(2-benzothiazolyl)-3-methyl-4-azo-pyrazil-5-one derivatives and their Cu(II) complexes. J Therm Anal Calorim. 2003;72(2):525–31.
44. Dincalp H, Toker F, Durucasu J, Avcibasi N, Icli S. New thiophene-based azo ligands containing azo methine group in the main chain for the determination of copper(II) ions. Dyes Pigment. 2007;75(1):11–24.
45. Chen Z, Wu Y, Gu D, Gan F. Nickel(II) and copper(II) complexes containing 2-(2-(5-substitued isoxazol-3-yl)hydrazono)-5,5-dimethylcyclohexane-1,3-dione ligands: synthesis, spectral and thermal characterizations. Dyes Pigment. 2008;76(3):624–31.
46. Rotaru A, Moanta A, Salageanu I, Budrugeac P, Segal E. Thermal decomposition kinetics of some aromatic azomonoethers. Part I. Decomposition of 4-[(4-chlorobenzyl)oxy]-4′-nitro-azobenzene. J Therm Anal Calorim. 2007;87(2):395–400.
47. Rotaru A, Kropidlowska A, Moanta A, Rotaru P, Segal E. Thermal decomposition kinetics of some aromatic azomonoethers. Part II. Non-isothermal study of three liquid crystals in dynamic air atmosphere. J Therm Anal Calorim. 2008;92(1):233–8.
48. Rotaru A, Moanta A, Rotaru P, Segal E. Thermal decomposition kinetics of some aromatic azomonoethers. Part III. Non-isothermal study of 4-[(4-chlorobenzyl)oxy]-4′-chloro-azobenzene in dynamic air atmosphere. J Therm Anal Calorim. 2009;95(1):161–6.
49. Barbera J, Giorgini L, Paris F, Salatelli E, Tejedor RM, Angiolini L. Supramolecular chirality and reversible chiroptical switching in new chiral liquid-crystal azopolymers. Chem Eur J. 2008;14(35):11209–21.
50. Benmouna R, Benyoucef B. Thermophysical and thermomechanical properties of Norland Optical Adhesives and liquid crystal composites. J Appl Polym Sci. 2008;108(6):4072–9.
51. Chao TY, Chang HL, Su WC, Wu JY, Jeng RJ. Nonlinear optical polyimide/montmorillonite nanocomposites consisting of azobenzene dyes. Dyes Pigment. 2008;77(3):515–24.
52. Lu M, Cunningham BT, Park SJ, Eden JG. Vertically emitting, dye-doped polymer laser in the green (lambda similar to 536 nm) with a second order distributed feedback grating fabricated by replica molding. Opt Commun. 2008;281(11):3159–62.
53. Oliveira-Campos AMF, Oliveira MJ, Rodrigues LM, Silva MM, Smith MJ. Thermal analysis of a polymorphic azo dye derived from 2-amino-5-nitrothiazole. Thermochim Acta. 2007;453(1):52–6.
54. Galikova A, Pola J. Highly sensitive TGA diagnosis of thermal behaviour of laser-deposited materials. Thermochim Acta. 2008;473:54–60.
55. Emandi A, Jula N, Vasiliu C, Dinescu M, Constantinescu C, Calinescu M, Vasilescu M. Some aspects about the properties of nanostructured organotranzitional Cu(II) complex on a polymeric matrix as optical sensor. In: Proceedings of the international conference on microelectronics and computer Science—ICMCS Sep 19–21, 2007, Chisinau, Republic of Moldova; 2007. p. 84–87.
56. Kropidłowska A, Rotaru A, Strankowski M, Becker B, Segal E. Thermal stability and non-isothermal decomposition kinetics of a heteroleptic cadmium(II) complex, potential precursor for semiconducting CdS layers. J Therm Anal Calorim. 2008;91(3):903–9.
57. Tătucu M, Rotaru P, Rău I, Spînu C, Kriza A. Thermal behaviour and spectroscopic investigation of some methyl 2-pyridyl ketone complexes. J Therm Anal Calorim. 2010;100(3):1107–14.
58. Rotaru P, Scorei R, Hărăbor A, Dumitru MD. Thermal analysis of a calcium fructoborate sample. Thermochim Acta. 2010;506(1–2):8–13.
59. Grundner C, Poiesz K, Redman-Fuery N. Development and use of a TG-DTA-microscope for evaluation of pharmaceutical materials. J Therm Anal Calorim. 2006;85:91–8.
60. Gusakov A, Voropayev A, Zheludkevich M, Vecher A, Raspopov S. Studies of the interaction of copper with atomic and molecular oxygen. Phys Chem Chem Phys. 1999;5311–14.

61. Du H, Fuh R, Li J, Corkan A, Lindsey J. PhotochemCAD: a computer-aided design and research tool in photochemistry. Photochem Photobiol. 1998;68:141–2.
62. Herzinger C, Johs B, McGahan W, Paulson W, Woollam J. Ellipsometric determination of optical constants for silicon and thermally grown silicon dioxide via a multi-sample, multi-wavelength, multi-angle investigation. J Appl Phys. 1998;83:3323.
63. Ion V, Galca A, Scarisoreanu N, Filipescu M, Dinescu M. Spectroscopic ellipsometry study of amorphous $Sr_xBa_{1-x}Nb_2O_6$ thin films obtained by pulsed laser deposition. Phys Stat Sol. 2008;5:1180–3.